

Symphony: Optimized Model Serving using Centralized Orchestration

Lequn Chen*

Weixin Deng*

Anirudh Canumalla*

Yu Xin*

Matthai Philipose†

Arvind Krishnamurthy*

Abstract

The orchestration of deep neural network (DNN) model inference on GPU clusters presents two significant challenges: achieving high accelerator efficiency given the batching properties of model inference while meeting latency service level objectives (SLOs), and adapting to workload changes both in terms of short-term fluctuations and long-term resource allocation. To address these challenges, we propose Symphony, a centralized scheduling system that can scale to millions of requests per second and coordinate tens of thousands of GPUs. Our system utilizes a non-work-conserving scheduling algorithm capable of achieving high batch efficiency while also enabling robust autoscaling. Additionally, we developed an epoch-scale algorithm that allocates models to sub-clusters based on the compute and memory needs of the models. Through extensive experiments, we demonstrate that Symphony outperforms prior systems by up to 4.7x higher goodput.

1 Introduction

We consider the setting of a cloud-scale inference service that supports the scalable execution of a high-volume inference workload involving a large number of deep neural networks (DNN) models on a cluster of accelerators (e.g., GPUs). Such an inference service is increasingly needed to consolidate the machine learning needs of cloud services within a datacenter. An effective inference service has to not only provide high throughput for a diverse set of models but also has to provide results within tight latency bounds that are appropriate for user-facing cloud services. This challenging workload is further exacerbated by the increasing computing and memory requirements of newer DNN models.

In many respects, a cloud-scale inference service doesn't differ much from the traditional cloud service model as it would have to scalably balance incoming requests across backends, adapt to workload changes (i.e., autoscale), and achieve high execution efficiency without compromising on the desired latency bounds. In addition to these requirements, DNN inference imposes additional challenges on a cloud-serving platform. First, as DNNs use linear algebra operators, batched execution of DNN inferences improves the utilization efficiency of the accelerators. So, model inferences should be issued in batches, but the batches should be appropriately sized to prevent violations of latency SLOs. The batching strategy also needs to accommodate for both models with strong batching effect as well as those that have little to none.

Second, given the sizes of DNN models are typically large, an inference service has to carefully plan for memory and optimize the allocation of models to accelerators. In particular, the on-demand loading of models is challenging, especially given the tight latency SLOs for cloud services. Third, the system has to dynamically allocate resources to cope with changing workloads, and it can only do so if the underlying *batched scheduling* algorithm provides a robust signal on the degree of under-/over-provisioning of cluster resources. Taken together, these considerations pose new challenges for the load-balancing and scheduling algorithms employed by the cloud inference service.

Symphony is an inference-serving system that supports the consolidated execution of DNN models on a cluster of GPUs. It uses the following techniques to do so.

First, it employs a centralized dispatcher to schedule inference tasks on accelerators dynamically, dispatch a batched inference task to whichever accelerator is available, and maximize the statistical multiplexing of individual model workloads on accelerators. The centralized dispatcher is built as a scalable multi-core scheduling engine that can handle millions of requests by operating as a cluster-wide orchestrator without interposing on dataplane operations.

Second, the centralized dispatcher employs an online batch scheduler that amortizes batch invocation costs using a non-work-conserving algorithm that delays dispatching while preserving latency SLOs. The non-work-conserving scheduler also enables the predictable use of resources to provide precise information to a cluster autoscaling system to adapt to changing workloads.

Third, in order to effectively implement the delayed dispatch decisions of our non-work-conserving scheduler, we engineer the communication runtime system to leverage one-sided and two-sided RDMA to reduce the communication latencies of the dispatch path.

Finally, Symphony employs a periodic epoch-scale optimization algorithm that allocates models to GPU backends in order to balance computational loads while conforming to the memory capacity constraints of the accelerators.

Symphony differs from prior systems in substantial ways. Nexus [27] is the system that is most similar to that of Symphony in terms of functionality, as it is able to support the execution of a collection of DNN models while optimizing for cluster efficiency and automatically adapting to workload changes. Nexus, however, employs a distributed dispatch mechanism coupled with a static determination of execution schedules on each GPU for a given epoch. Our work demonstrates that a centralized scheduler can employ dynamic

*University of Washington

†Microsoft

scheduling algorithms to provide significantly higher inference throughput without violating latency SLOs. Another related system is Clockwork [6], which targets the predictable execution of inference tasks on a GPU cluster. Clockwork uses a centralized controller to funnel and distribute all inference requests (including their associated data inputs) from clients to backends, but its scheduling mechanism focuses on predictability as opposed to efficiency. In particular, our evaluations show that a work-conserving scheduler, such as the one provided by Clockwork, cannot maximize batch efficiency benefits, nor can it enable effective autoscaling. Our work shows that a non-work-conserving scheduling mechanism is required to both enable efficient use of GPU resources as well as continually adapt to workload conditions.

To support our design decisions, we employ a combination of analytical models and empirical microbenchmarks. Our evaluation includes extensive comparisons of Symphony with related systems, across a wide range of workloads. Our results demonstrate up to 4.7x performance gain in goodput. Symphony further differentiates itself from other systems by exhibiting ideal autoscaling properties that enable effective adaptation to workload changes.

2 Background on Inference Serving Systems

2.1 Inference Serving Workloads

We consider scheduling inference tasks comprising of DNN executions on accelerators, such as GPUs. DNNs are networks of linear algebra operations (e.g., matrix multiplication and convolution), called *layers* or *kernels*, where the networks are typically referred to as *models*. The execution characteristics of these DNN-model-based inference tasks have important implications for the design of inference serving systems. First, it is well known that the accelerator utilization achieved by kernels depends critically upon the extent of *batching*, i.e., grouping input matrices into higher-dimensional ones before applying custom “batched” implementations of the kernels. This form of batching allows accelerators to reduce the accelerator’s memory access costs many more times than without batching by operating one kernel on each loaded input. Second, DNN layers can be as large as tens to hundreds of MBs. Loading models into memory can cost tens to hundreds of milliseconds, and this argues for explicit pre-loading models to GPUs as opposed to on-demand loading within the confines of small latency SLOs.

In addition to the requirements specific to DNN serving, we also need to meet the traditional goals of a serving system. First, requests have to be satisfied within latency bounds that are set by the application service invoking the inference tasks. In the context of datacenter applications, e.g., serving ads or various forms of real-time detection tasks, the latency SLOs are typically in the order of a few tens of milliseconds and severely constrain the extent to which requests can be batched. Second, inference serving systems, as with other datacenter

services, would have to handle traffic changes on a time scale of dozens of minutes as well as tolerate finer-grained fluctuations that happen in real life. To tolerate micro-level fluctuation, serving systems would have to appropriately provision to handle bursts. Even with overprovisioning, when an extreme burst shows up, the serving system can still run out of capacity and drop or delay requests, as long as the percentage of affected requests is below a threshold specified in the service level agreement (e.g., 99% requests served within 20ms). We define *goodput* of a model serving system as the highest aggregate throughput over all models such that p99 tail latency of each model is less than their respective latency SLO.

2.2 Model Serving Systems

We now describe some canonical model serving systems, their design goals, and the techniques employed by them.

Clipper and TensorFlow Serving: The first generation of serving systems focused on a single model or a few models associated with a single application, as exemplified by Clipper [3] and Tensorflow Serving [20]. Clipper can serve a variety of ML models on CPUs and GPUs. Given a request to serve a machine learning task, Clipper selects the type of model to serve it, batches requests, and forwards the batched requests to a backend container. Clipper also provides approximation and caching services, which is complementary to our goals. Tensorflow Serving can be viewed as a variant of Clipper that does not provide approximation and caching but has additional machinery for versioning models. Just by their very designs, these systems don’t provide any statistical multiplexing benefits across models and applications. In fact, if multiple instances of these serving systems are run concurrently on the same set of GPUs, the execution could result in unexpected slowdowns and violations of SLAs due to interference across models.

Nexus: Nexus [27] represents the second generation of serving systems that are explicitly designed to support multiple models invoked by different applications and services. Nexus consolidates the models on a shared cluster in order to obtain performance gains from statistical multiplexing. Every epoch (which is in the order of minutes), Nexus uses a version of a bin-packing algorithm to allocate models to GPUs based on the load associated with the models and their latency SLOs. Frontends, running application logic, perform distributed load-balancing of inference tasks to the different GPUs hosting a given model. A GPU backend then performs a round-robin execution of batched inferences for models allocated to it. The backend engine running on each GPU uses a work-conserving scheduler to dispatch batches of currently accumulated requests during the round-robin execution.

In Nexus, the allocation of models to GPUs is performed at epoch boundaries based on the current load associated with different models. The system also performs epoch-level autoscaling to provision or release GPUs based on current loads.

During an epoch, models are statically partitioned across GPUs. Static partitioning simplifies system design and request routing, and the partition changes happen only as part of a control plane reconfiguration event. However, the partitioning and rigid allocation of GPUs to models means that each model needs to be overprovisioned for its high percentile demand to minimize request drops due to bursts, thus resulting in resource inefficiencies.

Clockwork: Clockwork [6] is another model serving system that consolidates a multi-model DNN workload on a shared cluster. Clockwork’s primary goal is the predictable execution of inference tasks, and it introduces a number of techniques to reduce the variability of execution costs across different stages of an inference task. Clockwork improves resource utilization by allowing requests of a model to run on any GPU; instead of having a static binding of models to GPUs, Clockwork allows models to be dynamically loaded if there is sufficient time to load the model given the model’s execution latency constraint. Clockwork performs this dynamic allocation of models to GPUs and scheduling of the inference tasks using a centralized controller that is on the data path of all requests sent from the frontends to the backends. The centralized controller assigns inference tasks to free backends, sometimes after performing an on-demand load of the corresponding model.

Clockwork uses consolidation as a technique to enhance execution predictability. Crucially, cluster efficiency and auto-scaling in response to workload changes are non-goals, with the cluster sized statically to accommodate the consolidated peak loads of the models. Our work exploits information that a centralized scheduler knows to make better schedules. Symphony provides scheduling algorithms that not only improve cluster efficiency but can also enable adaptation to workloads in a consolidated setting.

3 Motivating Experiments

In this section, we provide measurements that help guide the design of our model-serving system.

3.1 Benefits of Batch Amortization

We evaluate the batch amortization benefits for various DNN models. We execute varying batch sizes of each model, measure the execution cost, and then fit them into a linear model:

$$\ell(b) = \alpha b + \beta,$$

where β is the fixed cost of invoking a model on a batch of requests, and α is the cost of each additional task in the batch. Large batches amortize the fixed cost β and help achieve higher throughputs. (Our measurements indicate that the linear model provides an accurate fit for the execution latency.)

The collected data (presented in Table 1) shows the fixed cost could be significant (e.g., $\beta/\alpha > 2$ for most models), indicating that a scheduling algorithm should explicitly avoid the invocation of small batch sizes. An additional aspect of the

Model	α (ms)	β (ms)	β/α	F	S	D
DenseNet121	1.06	10.31	9.71	32	99	2172
EfficientNet	1.56	5.58	3.55	21	88	1519
InceptionV3	1.96	8.77	4.46	92	230	3386
MobileNet	1.01	2.39	2.36	17	84	2653
ResNet50	2.05	5.37	2.62	98	170	2798
VGG16	2.73	5.78	2.11	528	822	6200

Table 1: Model profiles on an NVIDIA 1080Ti. F: File size (MB); S: Static memory size (MB); D: Dynamic memory size (MB).

analysis is that the execution time is predictable and can be estimated based on the batch size. This lets us model the ideal throughput behavior of a DNN model under different batching configurations, which is helpful in designing an online scheduling algorithm that maximizes accelerator efficiency.

Implication: The fixed cost for invoking batches varies across models and is significant for most models. Scheduling algorithms need to take model characteristics into account in determining how to form batches and when to dispatch them.

3.2 Memory requirements of models

We next instrument some of our models in our model zoo to characterize the amount of GPU memory consumed by models. There are three different metrics of memory utilization: *model size* refers to the cumulative size of parameters associated with the model, *static memory* refers to the amount of static GPU memory occupied by the model when loaded onto a GPU, and *dynamic memory* refers to the additional dynamically allocated GPU memory when the model is used on a batch of inference tasks. The dynamic memory is deallocated when the inference batch completes execution.

The experimental data (again in Table 1) demonstrates that, while models are large, multiple models can reside on a modestly sized GPU. However, the dynamic memory allocated to a model can be substantially higher than its static size, indicating significant bloat-up during execution time. These results indicate that multiple models can be GPU-resident as long as we minimize the number of models that are actively operating on input data. In practice, strict time multiplexing of the GPU, wherein only one model is actively executing at a given point in time, lets us have a few tens of models loaded onto a GPU and provides us with sufficient flexibility in the dynamic scheduling decisions.

Implication: Each model can be pre-loaded on a subset, but not all of the cluster nodes, thus allowing for dynamic model dispatch to any one of the candidate backends and yielding statistical multiplexing benefits.

3.3 Downside of Distributed Scheduling

We now examine the operations of Nexus, a model serving system that distributes the inference routing decisions across multiple frontends. Nexus’s scheduling happens in three components: (1) A cluster allocator decides the models executed by each backend server, (2) frontend servers decide which backend server to route an incoming request to, and (3) backend servers decide which requests to be included in the next

Window	Avg. Req. Rate	mean(RPW)	Frontends	std(RPW)
400 ms	10000 rps	40 rps	1	0.753 rps
			25	2.463 rps
200 ms	2000 rps	4 rps	1	0.396 rps
			25	1.860 rps

Table 2: Statistical simulation shows that multiple frontends doing round-robin individually amplifies the fluctuations in request rate.

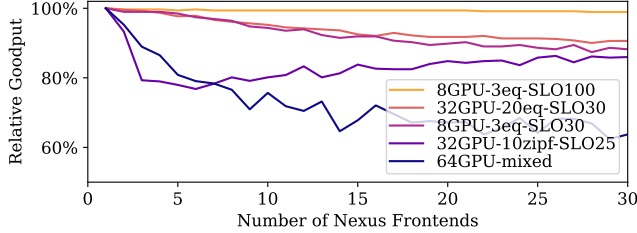


Figure 1: Distributed scheduling hurts goodput

batch. Since there is no coordination between frontend servers, multiple frontend servers might route requests to the same backend at the same time, essentially amplifying the burstiness of the request rate.

Table 2 shows a statistical experiment resembling a distributed scheduling design. “Clients” generates requests with Exponential distribution gaps to “frontends”. A “frontend” dispatches requests to one of 100 “backends” using round robin. And we count the number of requests a “backend” receives in a fixed time window (RPW), which is analogous to the number of requests queued up in a real backend. The two setups resemble a looser and a tighter latency-SLO-bound workload, respectively. The data shows that the standard deviation of RPW in the multi-frontend setup is several times higher than that in the single-frontend setup.

In addition to the typical short-term overloads on some nodes, there is also a reduction in GPU efficiencies on the remaining nodes due to the dispatch of small batches that have reduced levels of amortization of batching costs.

To understand the negative effect of distributed scheduling, we run Nexus with varying numbers of frontends. A single frontend can ensure that batches are dispatched uniformly, while increasing the frontends results in load skews and sub-optimal batches. We consider various workload setups, e.g., the number of GPUs varying from 8 to 64, the number of models varying from 1 to 37, and latency SLO varying from 20 to 100. As shown in Figure 1, using multiple frontends degrades the goodput of Nexus by 5% to 40% in various settings.

Implication: While a distributed scheduling system can scale well, the associated distributed dispatch can amplify burstiness and reduce batch efficiency in model serving systems.

4 Design and Implementation

In this section, we describe the design of Symphony and outline its core components and techniques.

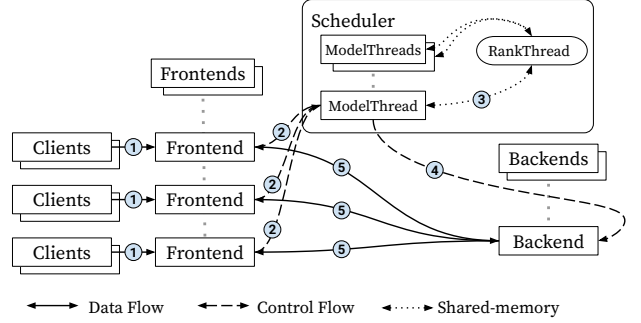


Figure 2: Symphony Architecture Design. Sequence number shows the journey of a batch.

4.1 System Overview

Symphony is designed to realize a high degree of GPU consolidation via statistical multiplexing of different types of inference tasks, high GPU efficiency through batched executions, and quick response to workload changes. It achieves these properties by using the following techniques.

Dynamic scheduling of model invocations on GPUs: We pre-load each model on more GPUs than what is required to support the measured load for the model. This allows us to dynamically select any available GPU that has the model loaded to execute a batch of model invocations.

Centralized scheduling off the datapath: We employ a centralized scheduler to match available GPUs with batches of inference tasks. The centralized scheduling is performed off the datapath.

Non-work-conserving schedules: The scheduler accumulates batches of inference requests and assigns them to backends in a non-work-conserving and delayed manner. The intentionally delayed schedule is designed to take advantage of batch amortization as well as provide robust signals to the auto-scaler that responds to workload changes.

System architecture: We now outline the overall system architecture and how the different system components work together (depicted in Figure 2). As with other model serving systems [6, 27], the frontends represent nodes that run application logic and invoke model inferences. Multiple frontends running the same or different applications can invoke inference tasks for the same model. The model inferences are performed in batches on a cluster of backends, each equipped with accelerators such as GPUs. The backends are grouped into different sub-clusters, where GPUs in the same sub-cluster have the same set of models loaded at a given time.

The centralized scheduler manages the scheduling of requests on the backends. The frontends communicate queued-up inference tasks and their deadlines to the scheduler; tasks are concisely represented using unique task IDs. The scheduler determines the batching of inference tasks and identifies the backend that will execute a given batch. The frontends then directly communicate the input data for the inference tasks to the selected backend.

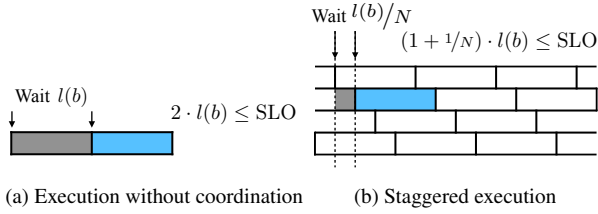


Figure 3: Demonstrations of the queuing delay.

Periodically, over epochs of a few minutes, Symphony performs the following tasks: allocating and loading models on sub-clusters of GPUs and autoscaling to react to workload changes. The centralized scheduler is architected to process millions of requests per second and manage tens of thousands of GPUs.

4.2 Centralized scheduler

Centralized scheduling brings three benefits. First, the scheduler can dynamically schedule batches of inference tasks to any one of the available backends to obtain statistical multiplexing benefits. In particular, it can balance out short-term variations in loads across different models. Second, a centralized scheduler can evenly distribute loads across successive dispatches of a model’s batches to various GPU workers. Third, a centralized scheduler can reduce the queueing delay for batches by accumulating just one active batch for each model type and funneling it to the next available GPU. This reduced queueing delay translates to being able to execute larger batches within the latency SLO and an increase in GPU efficiency.

We first present a centralized scheduling model, study the ideal batching behavior, and use it as a benchmark for our scheduling policies.

Ideal Batching from Coordinated Execution. We examine a simple case of the scheduling problem where all requests are for a single model that is hosted on N backends. We also consider the ideal setting of requests arriving at uniform time intervals at a known rate, λ . Denote $\ell(b)$ as the execution latency of the DNN model with a batch size of b . Suppose each backend runs batch after batch without pausing. We model the time elapsed in processing a request as the queueing delay waiting for the next batch to be scheduled and the execution latency for a batch.

In a system such as Nexus that uses multiple frontends distributing requests to backends in an uncoordinated manner, the worst-case queueing delay could be as long as the batch execution latency. A request that arrives right after a previous batch starts has to wait for the batch to complete before getting scheduled as part of the next batch (Figure 3a). Therefore, the batch size b needs to satisfy the constraint:

$$2 \cdot \ell(b) \leq \text{SLO} \quad (1)$$

A centralized scheduler can coordinate the execution of backends and reduce queueing delays. With uniform arrival, the scheduler can realize a synchronized execution model,

where the N backends are staggered perfectly with $\ell(b)/N$ intervals (Figure 3b). Suppose the scheduler was to dispatch an incoming request to the earliest backend that will become available. In that case, the worst-case queueing delay reduces from $\ell(b)$ to $\ell(b)/N$. In addition to the SLO constraint, we also need to ensure that the total throughput delivered by N backends matches the request rate λ (Eqn. 3). Combining the two equations, we can solve for b and N .

$$(1 + 1/N) \cdot \ell(b) \leq \text{SLO} \quad (2)$$

$$N \cdot b / \ell(b) \geq \lambda \quad (3)$$

In a more general setting, such a stable state does not always hold due to request rate fluctuations and having a heterogeneous set of models. The b and N solved by Eqns. 2 and 3 serve two purposes. First, we use N to identify the number of GPU resources needed when a new model is introduced to the system or an epoch-level rebalancing operation is performed. Second, we use b and $\ell(b)/N$ as ideal benchmark values to compare the actual batch sizes and queueing delays realized by our scheduling algorithms in our evaluations.

4.3 Scheduling Algorithm

We now present the algorithm used by our centralized scheduler that is suited for request rate fluctuations and more realistic arrival patterns. Under non-uniform or random arrivals, the system will likely encounter cases where the queued-up model batches aren’t large when a GPU becomes available. These cases introduce a tradeoff. The scheduler could dispatch one of the batches immediately, keep the GPUs busy, but have reduced amortization of the batch’s fixed costs. Alternatively, the scheduler could let the GPU idle till the existing batch candidates become larger and execute a larger batch with better batch efficiency and greater amortization of the batch fixed costs. The former is a *work-conserving* schedule, while the latter is a *non-work-conserving* schedule that trades GPU idle time for greater GPU efficiency during execution. A key challenge is that the scheduler needs to navigate this trade-off in the context of a diverse set of models, with some having minimal fixed batch costs and others having high clinched batch costs.

The centralized scheduler maintains batches of queue inference tasks for different models and dispatches them to the backends. Our scheduling algorithm can be described as a set of policies that address the following questions: (1) when does a queued batch of tasks become *schedulable*, (2) which of the schedulable batches are sent to an available backend, and (3) which tasks in a batch are dropped if the batch cannot complete before its deadline.

Scheduler state: The scheduler maintains the following state associated with the different models.

- For each backend, the scheduler maintains the time that the backend will become idle (finish execution), **free_at**.
- For each model, the scheduler keeps updating a new **Candidate** set of requests for the upcoming batch.

- For each candidate, the scheduler computes a value (**sched_at**) that determines what is the latest time to which the candidate can be updated and still be scheduled to meet its deadline. We discuss below how that is computed.

Let **reqs** be a candidate and $|\mathbf{reqs}|$ be the number of requests currently associated with a candidate batch. Further, let $\mathbf{dl}(\mathbf{reqs})$ be the execution deadline for the earliest request after considering its latency SLO and network processing delays. We set **sched_at** as $\mathbf{dl}(\mathbf{reqs}) - \ell(|\mathbf{reqs}| + 1)$, where ℓ is the execution latency profile of the DNN model. We justify this as follows. If a request is received before $\mathbf{dl}(\mathbf{reqs}) - \ell(|\mathbf{reqs}|)$ but after $\mathbf{dl}(\mathbf{reqs}) - \ell(|\mathbf{reqs}| + 1)$, then the candidate cannot include this request and still finish before the deadline. This means that $\mathbf{dl}(\mathbf{reqs}) - \ell(|\mathbf{reqs}| + 1)$ is the latest time at which we can update the candidate to include a new request, and we set **sched_at** to be this value.

We now consider each of the scheduling questions outlined earlier and discuss different scheduling policy options.

When is a candidate schedulable? We outline two extreme options for this scheduling question. A candidate can be considered as schedulable as soon as: (1) the candidate is formed with its first request, (2) current time reaches **sched_at**.

The first policy option is work-conserving as a candidate can be dispatched to an available backend immediately. The second is non-work-conserving, as it might delay allocating a candidate to a backend even if one is available; it instead maximizes the batch execution size while avoiding dropping requests. We will further refine the second policy in order to handle models with different batching fixed costs after the following analysis that explores the underlying tradeoff.

Consider a single node repeatedly executing queued-up inference tasks of a given model and aiming to dispatch a batch of size k every cycle. Suppose fewer than this number of requests are queued up at the end of an execution cycle. In that case, the node can either execute this batch immediately or wait for additional tasks to arrive, resulting in the tradeoff between not incurring idle times and maximizing accelerator efficiency. If the batch amortization benefits are sufficiently high (i.e., β/α is large) and if the queued-up tasks are much less than k , then it might be profitable to be non-work-conserving. In addition to improving the efficiency of the next batch, it will ensure that there is a sufficient execution cost for the subsequent batch to build up to a healthy size.

The following analysis illustrates this trade-off. Denote the model’s latency profile as $\ell(b) = \alpha b + \beta$, and request arrival rate as λ . Suppose b requests are queued-up at the end of an execution cycle. In expectation, the node would have to wait for $1/\lambda$ time to accumulate one additional request and $\alpha(b+1) + \beta$ time to execute the batch. If it were to execute the tasks immediately, then it would execute the b requests in $\alpha b + \beta$ time. The per-task execution times for the non-work-conserving and work-conserving options are $(1/\lambda + \alpha(b+1) + \beta)/(b+1)$ and $(\alpha b + \beta)/b$, respectively.

Model	DenseNet121, InceptionV3, ResNet50V2, VGG16, Xception, Bert
#Models	8, 16, 24, 32, 48, 64
#GPUs:#Models	1.0, 1.5, 2.0, 2.5, 3.0, 3.5, 4.0
SLO (ms)	20, 25, 30, 40, 50
Burstiness	$\Gamma(.1), \Gamma(.2), \Gamma(.3), \Gamma(.5), \Gamma(.7), \Gamma(1.)$

Table 3: Configurations for scheduling policy microbenchmark with homogeneous models

One can then show that the non-work-conserving option has a lower cost per task if $b < \beta\lambda$. In other words, if the number of queued-up tasks is small (smaller than the number of tasks that would accumulate during the startup cost β), then it would be profitable to adopt a non-work-conserving strategy and wait for an additional request.

Given the above analysis, we distill a non-work-conserving policy that incorporates the batching characteristics of the model. We say that a candidate is schedulable if either one of the two conditions is met: (a) the batch has accumulated $\beta\lambda$ tasks, or (b) the current time has reached **sched_at**. If neither of the conditions are met, then the batch will not be scheduled even if an idle GPU is available. In contrast, the work-conserving policy marks a batch as schedulable as soon as it is formed.

Which of the schedulable candidates are dispatched to an available backend? If there are backends available when a candidate becomes schedulable, we dispatch the candidate immediately. Otherwise, when a backend becomes available, we must determine which of the schedulable candidates is to be allocated. Our policy is to pick the schedulable candidate with the earliest **sched_at**, as it has the most stringent deadline.

If a candidate cannot execute by its deadline, how do we prune the candidate? When a candidate batch of requests cannot be scheduled before its associated deadline, we need to prune the candidate batch. We identify a subset of the batch with the earliest deadlines that can still be scheduled together and completed in time. The remaining elements of the batch will be moved to a later candidate that will be scheduled separately. This is same as the pruning strategy used by systems such as Clipper [3].

We attached pseudo-code of the scheduling algorithm in Appendix C for reference.

Microbenchmark evaluation of scheduling policies

We now present microbenchmark setups and results of running our system configured with the work-conserving policy and the non-work-conserving policy.

We consider homogeneous-model setups where all models have the same latency profile and mixed model setups. Table 3 lists options for each configuration dimension. Models listed in Table 3 are ordered by descending batching effect (β/α ranging from 9.7 to 0.02). Mixed-model setup contains 35 different models in a single run. Details about these models are listed in Table 5 in Appendix. The time gap between request arrivals follows the Gamma distribution, with the shape vary-

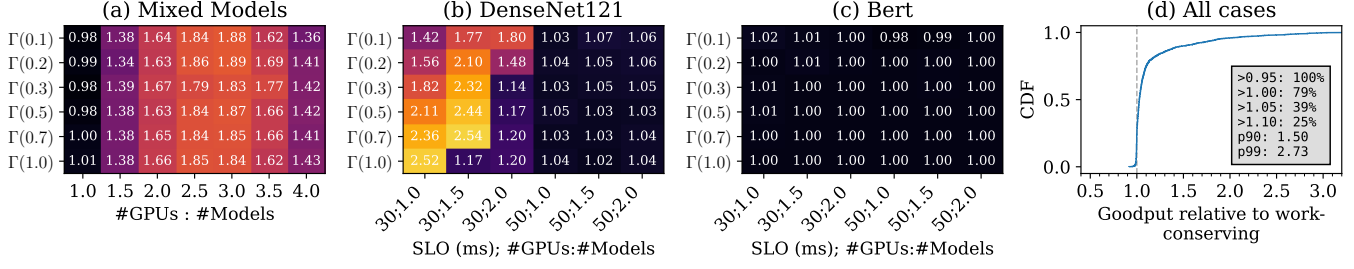


Figure 4: Goodput of the non-work-conserving policy relative to the goodput of the work-conserving policy

ing from 0.1 to 1.0. A smaller Gamma shape value represents a burstier request pattern. Notably, $\Gamma(1.0)$ is mathematically equivalent to the Exponential distribution, which means that the request rate follows the Poisson distribution.

Figure 4(a) shows that the non-work-conserving policy works very well when serving a mixture of models, gaining 34% to 89% higher goodput. Figure 4(b) examines a few cases with DenseNet121, which has strong batching effect. Our non-work-conserving policy shows 14% to 152% goodput increase under tighter latency SLO constraint (30ms). For looser latency constraint (50ms), the advantage is less prominent. The figure also shows that the non-work-conserving policy has bigger advantage under less bursty request rates, as burstier environment should favor the work-conserving policy. Figure 4(c) examines a few cases with Bert. Bert is a model with very weak batching effect, which should favor work-conserving policy. Our non-work-conserving policy achieves similar goodput to the work-conserving policy in these extreme cases. Figure 4(d) plots all cases. For nearly all cases, the non-work-conserving policy is no worse than (>0.95) the work-conserving policy. The non-work-conserving policy achieves 50% higher goodput for more than 10% cases and more than double in extreme cases.

4.4 Schedule Stability and Autoscaling

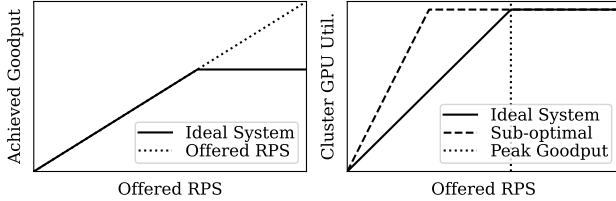


Figure 5: Ideal properties related to schedule stability and autoscaling.

We desire a certain form of schedule stability that will aid us in performing autoscaling in response to workload properties. In particular, we want our scheduler to exhibit the following two properties:

- Assume that the peak goodput of a cluster for a given workload is p . If we were to issue an offered load o higher than p , we would like our scheduler to have a bad rate comparable to $(o - p)/o$. Otherwise, under loaded conditions, the

system is exhibiting a goodput lower than the peak goodput, indicating a suboptimal congestion response.

- Given a peak goodput p , if we were to issue an offered load o lower than p , then we would like our scheduling system to have an average GPU idle time fraction comparable to $(p - o)/p$. (GPU idle time fraction is defined as the fraction of time the GPU spends idling without executing any tasks.)

We refer to these two properties together as a desired *flat-top* behavior, as illustrated in Figure 5. The flat-top behavior is desirable because a sudden burst in the aggregate load should not cause an undue increase in bad rate. More importantly, the scheduling system can then monitor the system performance signals of bad rate and GPU idle time to determine whether it needs to allocate or deallocate resources from the cluster. In our system, we periodically perform the following two actions:

Allocate GPUs: If the bad rate r is above a threshold, the autoscaler requests $N \cdot b / (1 - b)$ additional GPUs, where N is the current number of cluster GPUs.

Deallocate GPUs: If the GPU idle time fraction is f , then it deallocates $N \cdot f$ GPUs.

It is easy to achieve flat-top behavior when serving tasks that do not exhibit batch amortization benefits. However, when there are varying degrees of batch amortization across different candidates with different batch sizes, it is hard to get a robust signal for the autoscaling capability. For example, if a scheduler were to use sub-optimal batch sizes, then the GPU idle time would underestimate the true overprovisioning available in the system. Similarly, in overloaded conditions, the bad rate could provide an overestimate of additional resources required to achieve parity.

Schedule efficiency is intimately connected with having robust signals for adaptation. Symphony’s default scheduling policies that are non-work-conserving and maximize the batch amortization benefits are a good fit for providing the desired flat top behavior. We show in Section 5.3 that we achieve this behavior while a comparable system such as Clockwork exhibits a substantial loss in goodput as we increase the offered load beyond its capabilities. Further, we show that Clockwork’s work-conserving scheduler exhibits low GPU idle times even when the offered load is much lower than the peak load, thus preventing an autoscaling system

from reclaiming unnecessary GPU resources.

4.5 Scalability of centralized scheduler

At the scheduler, when we update a model candidate, we do not need to access other models’ information. On the other hand, backend availability is global information that all models need to access when trying to bind a candidate to a backend. For multi-core scalability, we separate the scheduler into two different kinds of entities.

A **ModelThread** accepts incoming requests to a particular model. It accesses only model-local information and updates the candidate. It then sends the candidate to **RankThread**.

The **RankThread** organizes the global information, i.e., backend availability and each model candidate’s timer. When a model’s timer rings, it checks whether there is a backend able to bind to the model’s candidate. If so, it grants the backend to the model and marks the backend as unavailable.

When the corresponding **ModelThread** receives the granted backend, it updates the candidate, finalizes it with the backend, and sends out the candidate batch to the backend immediately. It also informs the **RankThread** about when the backend will become available. It then registers a new candidate, containing tasks for the next inference batch, with the **RankThread**.

With this design, the centralized scheduler can utilize multiple independently executing **ModelThreads** spread across multiple cores. The **RankThread**, however, is shared by the different **ModelThreads** and represents the bottleneck in the system. Note that although a **ModelThread** needs to keep up with the request line rate, **RankThread** only need to be fast enough to keep up with the start and the finish events of GPU execution. Since the GPU execution is batched, usually with batch sizes larger than 10, the process rate for **RankThread** is an order of magnitude lower. Besides, we have engineered the system to have a limited amount of ranking logic on the **RankThread**, and a single **RankThread** is able to support dozens of **ModelThreads**. Thus, Symphony can scale to millions of requests per second.

4.6 Low latency data plane and Backend

Since a backend can fetch input data from frontends only after the scheduler has made the batch plan, it is critical to have a low-latency connection between frontends and backends. We use one-sided RDMA READs initiated from the backend to fetch inference inputs from the frontends. The networking behavior is studied in detail in Section 5.5.

Besides reading inputs, preprocessing inputs (e.g., decoding images) also takes a significant amount of CPU time. In our design, we choose to do preprocessing at frontends for two reasons. One is that the cluster can easily add CPU computation power by adding more frontends. More importantly, Symphony can then overlap the preprocessing time with the request’s queueing time instead of introducing an additional delay at the backends before GPU computations.

4.7 Partitioning Models

At epoch-scale granularity, we invoke a global partitioning algorithm that is used for two purposes: (1) Given a cluster and a set of models to be served from the cluster, we subdivide the cluster into multiple sub-clusters and an associated set of models for each sub-cluster. We then ensure that each backend in a sub-cluster is pre-loaded with all of the models associated with the sub-cluster. This ensures that any of the backends in a sub-cluster can execute any associated models and increases the ability to perform statistical multiplexing. Note that a single centralized coordinator is still responsible for scheduling all sub-clusters. (2) If the overall workload exceeds the scheduling capabilities of a centralized server, we partition the entire workload and the set of models across multiple clusters, each equipped with its own centralized coordinator. The two different partitioning algorithms are similar and are performed in a hierarchical manner every epoch, with the top-level algorithm partitioning the workload across clusters and the bottom-level algorithm partitioning across sub-clusters. We present below the bottom-level partitioning algorithm, as the top-level partitioning algorithm is a slightly simpler variant.

There are currently two constraints to be considered in partitioning a set of models across multiple sub-clusters, the combined request rate handled by a sub-cluster and the total size of all models associated with a sub-cluster. The first constraint represents a bound on the dispatching speed of a **RankThread** within a controller, as it has to handle all requests sent to a given sub-cluster. The second constraint is that each backend associated with a sub-cluster needs to load all of the sub-cluster’s associated models into bounded GPU memory.

To address these constraints, we decide to distribute the workload at the granularity of models. In particular, we partition the set of all models in the system into many disjoint sets of models, with each associated with a sub-cluster and managed by a corresponding dispatcher thread on the centralized scheduler. The benefit of such a design is that each dispatcher thread can function independently, so no communications between dispatcher threads are needed.

Aside from these constraints, we would like each dispatcher to have a relatively balanced set of models in terms of combined request rates and total size. Because the set of models and their request rates can change over time, we also want to minimize the disruption of such changes on the partition because backends won’t be able to process requests during the loading and unloading of models. In order to find a particular partition, we formulated the following mixed integer linear programming (MILP) model. Appendix A provides details on the MILP and an evaluation of its effectiveness.

5 Evaluation

We implemented Symphony in C++ with 10k lines of code. We use TensorFlow v2.5.0 as the engine to run DNNs. All

models are profiled with all different batch sizes to obtain actual execution latency.

We ran most evaluations in a 9-machine cluster. Each machine has two sockets of Intel Xeon E5-2690 v4 CPU (28 physical cores in total) and 64GB memory. The cluster is interconnected by 56Gbps Infiniband with Mellanox ConnectX-3 network interface card. 8 of the machines are equipped with one NVIDIA GeForce 1080Ti GPU on each machine, and the other machine without a GPU is used as the scheduler.

The same cluster is also used to emulate bigger clusters of more GPUs and faster GPU cards. Since the execution time of DNNs on GPU is highly predictable, we emulate the execution by simply introducing a delay at the backend. The introduced delay times are based on model profiles from 1080Ti and A100. We implemented the emulation mechanism for Symphony, Clockwork, and Nexus.

Clockwork uses TVM as the engine to run DNNs. In the experiments, we found that the TVM version shipped with Clockwork runs significantly slower than TensorFlow. To minimize the impact of different DNN execution engines, we always use emulated GPUs based on the profiling results on TensorFlow in Clockwork’s end-to-end experiments. Due to the limitation of TVM, Clockwork only supports power-of-two batch sizes. To make comparisons fairer, we added support for arbitrary batch sizes to Clockwork. Clockwork routes all input data through their centralized controller, which becomes a bandwidth bottleneck. To make comparisons fairer, we omit transferring input data for Clockwork.

We used multiple workloads to evaluate our system and baseline systems. Workloads differ in the following dimensions: (a) batching profiles of the models, (b) latency SLOs, (c) invocation popularity across models, (d) request arrival patterns, and (e) changes in the average request rate.

Our evaluation answers the following questions:

- How is the scheduling quality of Symphony under different kinds of workloads?
- Do end-to-end behaviors conform to the scheduler’s view?
- Where do performance benefits come from?
- How does Symphony differ from other systems?
- Can Symphony work with cluster auto scaling tools?
- Will the centralized scheduler become a bottleneck?
- What is the impact of low-latency, one-sided RDMA?
- Does Symphony respond to fast changing workloads?

5.1 End-to-end Goodput

We collected a mixed model zoo consisting of 37 widely-used DNN models, including variants of DenseNet [13], EfficientNet [31, 32], Inception [29, 30], MobileNet [9, 10, 26], NASNet [36], ResNet [7, 8], VGG [28], Xception [2], SSD-MobileNet [17], and Bert [5]. These models span a wide range of parameter sizes and execution speeds. Latency SLOs of models vary from 20 to 400 milliseconds. Batching charac-

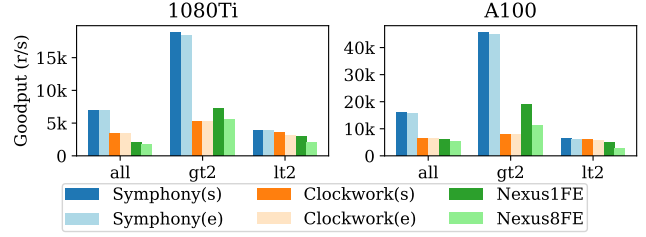


Figure 6: Goodput comparison among systems in mixed model zoo with different batching characteristics.

teristics of each model also differ. The full list of models and latency SLO is available in Table 5 and Table 6 in Appendix.

We evaluated Symphony, Clockwork, and Nexus on the mixed model zoo with 64 emulated GPUs in two separate clusters with NVIDIA 1080Ti and A100, respectively. Since both Symphony and Clockwork take the centralized approach, we ran both systems with both scheduler-only (s) and end-to-end (e) configurations. Scheduler-only runs only the scheduler and the load generator sends requests in the same process. The end-to-end configuration runs the scheduler, frontends, backends, load generators on separate machines. Since Nexus frontends take part in scheduling, we run Nexus with a single frontend and eight frontends, respectively, to observe the overhead of distributed scheduling.

Based on batching characteristics, we run the experiment in three settings: *all* runs all models listed in the model zoo; *gt2* runs models whose $\beta/\alpha > 2$, i.e., models that have strong batching effect; *lt2* runs models whose $\beta/\alpha < 2$, i.e., models that do not benefit much from batching.

The goodput of each system is shown in Figure 6. Comparing the goodput between (s) and (e), we can see that both Symphony’s and Clockwork’s schedulers have good control over the cluster and are able to predict the end-to-end performance. Comparing Nexus1FE and Nexus8FE, we observe 11% to 45% goodput loss from distributed scheduling.

When running all models, Symphony shows 2x to 2.4x the goodput of the baseline systems. When running models with strong batch effects, Symphony shows 3.5x the goodput of the baseline systems for 1080Ti and 5.7x for A100. These results indicate that Symphony produces better scheduling quality. It is worth pointing out that the advantage of Symphony is less prominent when running models with little batching effect. Symphony goodput is 23% and 10% higher in the 1080Ti cluster and the A100 cluster, respectively, in the *lt2* setup.

5.2 Scheduling Quality

We test Symphony’s scheduling quality under various workload characteristics. Then using two setups as examples, we take a closer examination to understand why Symphony achieves better scheduling quality.

5.2.1 Varying the workload characteristics

To evaluate Symphony’s scheduling quality across broader use cases, we conducted experiments with changes in three dimensions of workloads: latency SLO, model popularity,

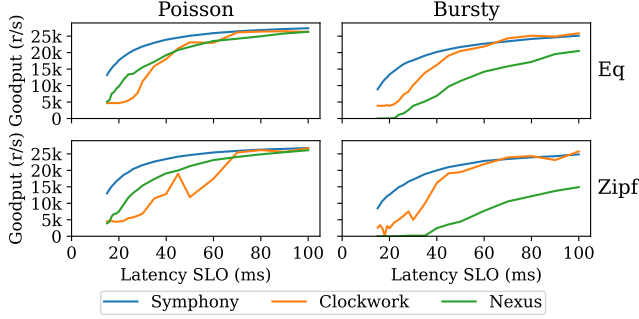


Figure 7: Effect of workload characteristics on goodput

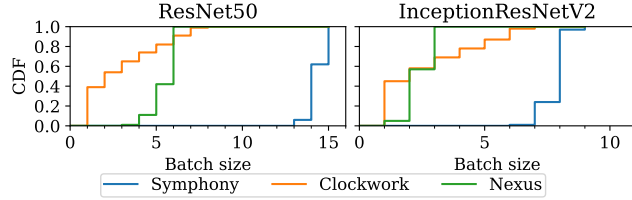


Figure 8: Batch size distribution

and request arrival. The experiments use 20 models whose batching profile is similar to ResNet50; this would represent specialized variants of the model for different applications [11, 22, 23]. All models are set to the same latency SLO, varying from 15ms to 100ms across data points. Popularity among models has two options: evenly popular or Zipfian distribution with a shape of 0.9. The time gap between requests also has two options: Exponential distribution (i.e., the request rate follows a Poisson distribution) or Gamma distribution with shape 0.05 (i.e., bursty request rate). 32 emulated GPUs are used in the experiments.

Figure 7 shows the goodput of the different systems under the various combinations of the experimental setups. Our findings include: 1) Symphony provides significant benefits in the tight-SLO cases across all four setups, and this is because Symphony optimizes for batch size while meeting SLOs. 2) Nexus does not work well with bursty workloads because of the static partitioning of models to backends; it does not enjoy the statistical multiplexing benefits of the other systems. 3) Loose-SLO cases are less challenging, with both Symphony and Clockwork producing good schedules. This is because the batch sizes are large; therefore, the marginal throughput improvements from higher batch sizes are small.

5.2.2 Batch Size

To understand how batch size affects goodput and to study how close is the batching behavior to the ideal staggered execution, we run a single copy of ResNet50 [7] and InceptionResNetV2 [29] separately with 8 GPUs on Symphony, Clockwork, and Nexus. Requests arrive in a Poisson distribution. The details of the models and the goodput on each system are listed in Table 4, and the distribution of batch size is shown in Figure 8.

Section 4.2 described the difference between backends executing independently without coordination and backends

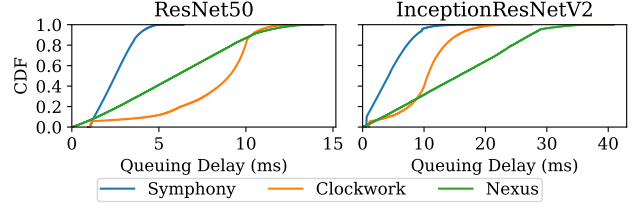


Figure 9: Queuing Delay

with staggered executions. Assuming requests arrive uniformly, the analytical solution of batch size can be calculated as $\lfloor (SLO/2 - \beta) / \alpha \rfloor$ and $\lfloor (SLO/(1+1/N) - \beta) / \alpha \rfloor$, respectively. Given batch size b , the throughput of N GPUs can be calculated as $Nb/(\alpha b + \beta)$.

Table 4 shows the calculation of the analytical batch size and throughput for both models for the two execution approaches. The data shows that the staggered execution can run with twice the batch size and achieve 30% ~ 50% higher throughput compared to execution without coordination. The empirical measurement shows that the goodput of Symphony is close to the analytical throughput of staggered execution, and the goodput of Nexus is close to the analytical throughput of execution without coordination. The difference between the real system and analytical calculation comes from differences in request arrival patterns and delays in real systems.

Figure 8 shows the batch size distribution. When running ResNet50, the majority of requests run with batch sizes greater than 14 and 6 for Symphony and Nexus, respectively. When running InceptionResNetV2, most batch sizes are greater than 8 and 3, respectively. The empirical measurement of batch sizes is close to the analytical solutions. Thus, the experiment confirms that Symphony’s scheduler generates batches whose sizes are close to that of the optimal staggered execution and thereby achieves high goodput. Figure 8 also explains why Clockwork’s goodput is low. The design of Clockwork’s scheduling algorithm does not optimize for large batch sizes. Clockwork’s algorithm picks an execution candidate merely based on the deadline, not taking batch size into account. Thus the probability of Clockwork choosing a specific batch size is uniform. Figure 8 shows this phenomenon for batch sizes greater than one.

5.2.3 Queuing Delay

Figure 9 shows the queuing delay in the same experiment as the last one. Queuing delay of a request is defined as the duration starting from the system receiving the request to a GPU initiating a batch containing the given request. Symphony’s queuing delay is 2x to 3x shorter than baseline systems, allowing more SLO budget to spend on execution. The longest queuing delay in Nexus is around half the latency SLO, due to its lack of coordination, as analyzed in Figure 3a. Although Clockwork uses a centralized scheduler, its longest queuing delay does not improve over Nexus in the ResNet50 case.

GPUs	Model	α (ms)	β (ms)	SLO	NoCoordination		StaggeredExec		Goodput (r/s)		
					BS	Throughput	BS	Throughput	Symphony	Clockwork	Nexus
8	[7]	1.053	5.072	25ms	7	4501 r/s	16	5839 r/s	5169	2036	3965
8	[29]	5.090	18.368	70ms	3	713 r/s	8	1083 r/s	907	482	590

Table 4: Analytical analysis of batching and empirical measurement of goodput. (BS: Batch Size)

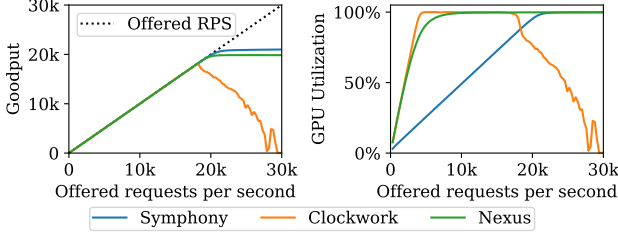


Figure 10: (Left) Stability. (Right) GPU Cluster Utilization

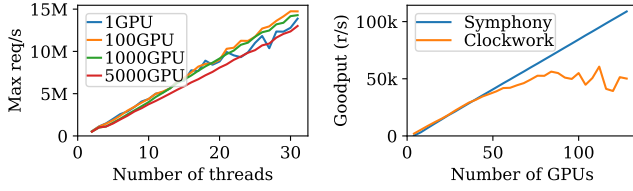


Figure 11: (Left) Symphony scheduler multicore scalability. (Right) Goodput varying the number of GPUs.

5.3 Auto Scaling

We study whether our system and baseline systems can provide robust signals to cluster auto-scaling tools. For the following two experiments, we use 10 ResNet models with 100ms latency SLO and uniformly popular Poisson request rate. We ran the test with 24 emulated GPUs.

Stability. We look at how systems behave when overloaded. Ideally, a model serving system should provide a stable goodput even when the offered request rate exceeds the cluster’s maximum capacity. Figure 10 (Left) shows that both Symphony and Nexus have flat-top behavior because both systems try to maintain a desirable batch size. Clockwork’s greedy algorithm, on the other hand, picks the next batch merely based on the top result ordered by a candidate’s earliest execution time and often dispatches small batches that are close to their deadlines. As shown in the graph, Clockwork’s goodput starts to degrade as soon as the system is overloaded. This unstable goodput makes it hard to perform autoscaling.

GPU Cluster Utilization. Figure 10 (Right) measures GPU cluster utilization as the sum of GPU busy cycles divided by the experiment duration divided by the number of GPUs. Both Clockwork and Nexus reach full GPU busy levels before reaching their respective peak goodput, indicating that both systems run with suboptimal batches. Symphony’s GPU utilization gradually increases and reaches full GPU busy level at near peak goodput, which means that Symphony has the capability to consolidate GPU usage. Hence, GPU utilization of Symphony is a good signal to cluster autoscaling tools.

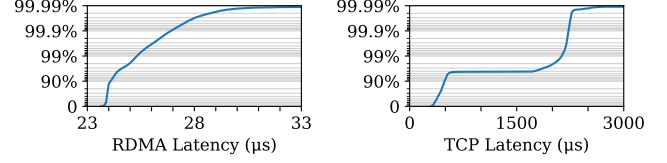


Figure 12: RDMA and TCP tail latency

5.4 Scalability

Since the centralized scheduler is involved in all requests, we want to ensure that it can keep up with the line rate. Figure 11 (Left) measures the maximum request rate that the Symphony scheduler can handle on a 32-core AMD EPYC 7502 CPU. We run this particular benchmark with the scheduler alone, without sending network messages or running GPUs. Requests and GPUs in these benchmarks are in-process objects used by the scheduler. Since there is no information exchange between **ModelThreads**, we observe that the throughput increases linearly with the number of threads. The plot also proves that the single-threaded **RankThread** is not a bottleneck. Although **ModelThreads** produces Candidates at line rate, **RankThread** only needs to pick up the latest candidate from **ModelThreads**. Therefore, a single **RankThread** has no problem handling dozens of **ModelThreads**.

Figure 11 (Right) serves 20 equally popular ResNet-like models with 100ms SLO. Symphony’s goodput increases linearly with the number of emulated GPUs. On the other hand, Clockwork was not designed for multicore scalability, and its use of locks on critical paths limits the overall throughput.

5.5 Impact of network

This subsection quantifies the benefits of using RDMA-based communications in Symphony. We first study the performance difference between RDMA and TCP. We ran a network incast benchmark among eight servers. The incast behavior is a good representation of sending inputs of a batch from frontends to the executing backend. The benchmark concurrently reads eight objects of 150KB from each server. RDMA tail latency was measured on 56Gbps Infiniband. TCP tail latency was measured on 40Gbps Ethernet.

Figure 12 shows the incast benchmark result. The lowest RDMA latency is within 24 μ s, which is very close to the theoretical lower bound of 21.5 μ s. The 99.99-th percentile latency in the RDMA network is within 33 μ s. Thus RDMA network is both low-latency and highly predictable. TCP, on the other hand, is not only slower but also has a very long tail. The 99.99-th percentile latency is 12x the median.

Then we study how network latency affects the model serving goodput. We run a workload consisting of 20 evenly popular models of similar batching profiles on an emulated 32-

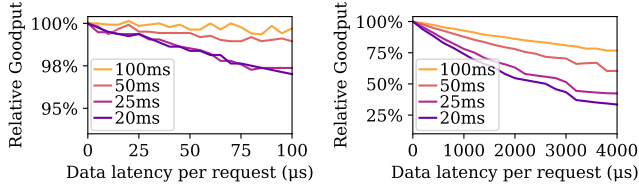


Figure 13: Effect of network latency on model serving goodput. (Left) within RDMA range. (Right) within TCP range.

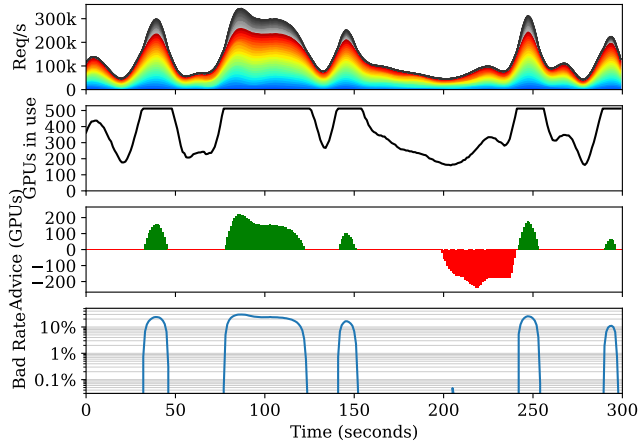


Figure 14: A changing workload on a 512-GPU cluster

GPU cluster with four settings of latency SLO: 20ms, 25ms, 50ms, and 100ms. Figure 13 (Left) shows that the network latency within the RDMA range only marginally reduces goodput. Figure 13 (Right) shows that network latency within the TCP tail latency range significantly hurts goodput. We observe that the tighter the latency SLO is, the more severely the goodput is impacted by network latency. This is because the data fetch occurs in the critical path of the scheduling dispatch. A GPU cannot start execution until all inputs in the batch are transferred to the backend. The longer the network latency is, the longer the GPU has to wait. The scheduler always uses the high percentile bound of network latency as the network delay estimation and would have to make earlier dispatch decisions. Therefore, unpredictable and high latencies lead to a significant decrease in the goodput.

5.6 Large cluster and changing workload

Lastly, we evaluate our system in a large cluster setup with a changing workload. The emulated cluster consists of 512 GPUs. The workload consists of 24 models with different batching characteristics and different SLOs. The request rate for each model is synthesized from 150 hours of videos.

Figure 14 shows the result. Color in the first subplot represents the goodput for each model. Grayscale in the first subplot shows the unsatisfied requests for each model. The stacked graph in total shows the overall request rate per second. The second subplot shows the number of GPUs used in the system. Symphony is able to consolidate GPU usage when the cluster is underloaded. The third subplot shows Symphony’s advice to the cluster’s autoscaling system in terms of

adding or removing GPUs. The fourth subplot shows the bad rate. Symphony is able to maintain a low bad rate when the cluster is not overloaded.

6 Related work

Model Serving Systems: Earlier, we described Symphony’s relationship to serving systems such as Nexus [27], Clockwork [6], Clipper [3], and Tensorflow Serving [20]. In addition, Salus [34] is a recent system that emphasizes loading multiple models into the GPU memory, but it mainly focuses on training and only discusses inference on a single-machine setup. INFaaS [24] focuses on model selection, trading off between the inference latency and the DNN model accuracy, which is in a different scope from ours. Perseus [16] is a good motivational paper for multi-tenant model serving, but they didn’t dive deep into scheduling algorithms. Our paper proposes a solution in this direction. Pretzel [15]’s most important technique is sharing layers across models. We believe that Symphony’s techniques can be extended to batch invocations of shared layers as well. Mark [35] and Morphling [33] focus more on autoscaling and machine provisioning. Our scheduler’s statistics and autoscaling advice can be good signals to these cluster management tools. Llama [25] and Scrooge [12] focus more on complex query pipelines whereas we focus on the batching efficiency of individual models. These systems can adopt our techniques to further improve the efficiency of individual models in a pipeline. MARK, Morphling, and Llama try to cut down costs on cloud infrastructures by choosing the right VMs/accelerators; our work is orthogonal and aims at improving the efficiency of the chosen target.

Load Balancing: Load balancing traffic in the cloud has been studied extensively, and many algorithms have been proposed to maximize throughput and minimize response time. There are two categories of algorithms: static load balancing algorithms (e.g., consistent hashing [14], and CFS [4]) distribute requests based on the prior knowledge of the capability of a node, while dynamic load balancing algorithms (e.g., the power of two choices [19], Distcache [18], and Sparrow [21]) take account into the run-time properties collected of nodes. Notably, Slicer [1] is a production-grade auto-sharder. However, Slicer does not apply to our use case because we have a tighter bound of latency SLO, and by Slicer’s distributed nature, it will result in a less balanced load.

7 Conclusion

We present the design of Symphony, a cluster-scale model serving system that can serve the consolidated demands of multiple machine learning applications. Our system uses a centralized dynamic scheduler (engineered to be off the data-path) to leverage the capabilities of fast networks and orchestrate the efficient execution of inference tasks on a cluster of accelerator-equipped backends. Our system relies on multiple techniques to achieve high efficiency, controller scalability, and responsiveness to workload changes. We provide

a non-work-conserving scheduling policy, effectively split the scheduling logic across a multi-core controller, and devise epoch-scale load and memory allocation algorithms for effective partitioning. Our resulting system achieves more than 4.7x higher performance than comparable systems, exhibits predictable behavior under overloaded conditions, and responds to workload changes in a timely manner.

References

- [1] Atul Adya, Daniel Myers, Jon Howell, Jeremy Elson, Colin Meek, Vishesh Khemani, Stefan Fulger, Pan Gu, Lakshminath Bhuvanagiri, Jason Hunter, et al. Slicer: Auto-sharding for datacenter applications. In *12th USENIX Symposium on Operating Systems Design and Implementation (OSDI 16)*, pages 739–753, 2016.
- [2] François Chollet. Xception: Deep learning with depth-wise separable convolutions. *CoRR*, abs/1610.02357, 2016.
- [3] Daniel Crankshaw, Xin Wang, Giulio Zhou, Michael J. Franklin, Joseph E. Gonzalez, and Ion Stoica. Clipper: A low-latency online prediction serving system. In *14th USENIX Symposium on Networked Systems Design and Implementation, NSDI 2017, Boston, MA, USA, March 27-29, 2017*, pages 613–627. USENIX Association, 2017.
- [4] Frank Dabek, M Frans Kaashoek, David Karger, Robert Morris, and Ion Stoica. Wide-area cooperative storage with cfs. *ACM SIGOPS Operating Systems Review*, 35(5):202–215, 2001.
- [5] Jacob Devlin, Ming-Wei Chang, Kenton Lee, and Kristina Toutanova. Bert: Pre-training of deep bidirectional transformers for language understanding. *arXiv preprint arXiv:1810.04805*, 2018.
- [6] Arpan Gujarati, Reza Karimi, Safya Alzayat, Wei Hao, Antoine Kaufmann, Ymir Vigfusson, and Jonathan Mace. Serving dnns like clockwork: Performance predictability from the bottom up. In *14th USENIX Symposium on Operating Systems Design and Implementation (OSDI 20)*, pages 443–462. USENIX Association, November 2020.
- [7] Kaiming He, Xiangyu Zhang, Shaoqing Ren, and Jian Sun. Deep residual learning for image recognition. *CoRR*, abs/1512.03385, 2015.
- [8] Kaiming He, Xiangyu Zhang, Shaoqing Ren, and Jian Sun. Identity mappings in deep residual networks. *CoRR*, abs/1603.05027, 2016.
- [9] Andrew Howard, Mark Sandler, Grace Chu, Liang-Chieh Chen, Bo Chen, Mingxing Tan, Weijun Wang, Yukun Zhu, Ruoming Pang, Vijay Vasudevan, Quoc V. Le, and Hartwig Adam. Searching for mobilenetv3, 2019.
- [10] Andrew G. Howard, Menglong Zhu, Bo Chen, Dmitry Kalenichenko, Weijun Wang, Tobias Weyand, Marco Andreetto, and Hartwig Adam. Mobilenets: Efficient convolutional neural networks for mobile vision applications. *CoRR*, abs/1704.04861, 2017.

- [11] Jeremy Howard and Sebastian Ruder. Universal language model fine-tuning for text classification. In *Annual Meeting of the Association for Computational Linguistics*, 2018.
- [12] Yitao Hu, Rajrup Ghosh, and Ramesh Govindan. Scrooge: A cost-effective deep learning inference system. In *Proceedings of the ACM Symposium on Cloud Computing*, SoCC '21, page 624–638, New York, NY, USA, 2021. Association for Computing Machinery.
- [13] Gao Huang, Zhuang Liu, and Kilian Q. Weinberger. Densely connected convolutional networks. *CoRR*, abs/1608.06993, 2016.
- [14] David Karger, Eric Lehman, Tom Leighton, Rina Panigrahy, Matthew Levine, and Daniel Lewin. Consistent hashing and random trees: Distributed caching protocols for relieving hot spots on the world wide web. In *Proceedings of the twenty-ninth annual ACM symposium on Theory of computing*, pages 654–663, 1997.
- [15] Yunseong Lee, Alberto Scolari, Byung-Gon Chun, Marco Domenico Santambrogio, Markus Weimer, and Matteo Interlandi. Pretzel: Opening the black box of machine learning prediction serving systems. In *13th {USENIX} Symposium on Operating Systems Design and Implementation ({OSDI} 18)*, pages 611–626. USENIX Association, 2018.
- [16] Matthew LeMay, Shijian Li, and Tian Guo. Perseus: Characterizing performance and cost of multi-tenant serving for cnn models, 2020.
- [17] Wei Liu, Dragomir Anguelov, Dumitru Erhan, Christian Szegedy, Scott Reed, Cheng-Yang Fu, and Alexander C Berg. Ssd: Single shot multibox detector. In *European conference on computer vision*, pages 21–37. Springer, 2016.
- [18] Zaoxing Liu, Zhihao Bai, Zhenming Liu, Xiaozhou Li, Changhoon Kim, Vladimir Braverman, Xin Jin, and Ion Stoica. Distcache: Provable load balancing for large-scale storage systems with distributed caching. In *17th USENIX Conference on File and Storage Technologies (FAST 19)*, pages 143–157, 2019.
- [19] Michael Mitzenmacher. The power of two choices in randomized load balancing. *IEEE Transactions on Parallel and Distributed Systems*, 12(10):1094–1104, 2001.
- [20] Christopher Olston, Noah Fiedel, Kiril Gorovoy, Jeremiah Harmsen, Li Lao, Fangwei Li, Vinu Rajashekhar, Sukriti Ramesh, and Jordan Soyke. Tensorflow-serving: Flexible, high-performance ml serving. *arXiv preprint arXiv:1712.06139*, 2017.
- [21] Kay Ousterhout, Patrick Wendell, Matei Zaharia, and Ion Stoica. Sparrow: distributed, low latency scheduling. In *Proceedings of the Twenty-Fourth ACM Symposium on Operating Systems Principles*, pages 69–84, 2013.
- [22] Sinno Jialin Pan and Qiang Yang. A survey on transfer learning. *IEEE Transactions on Knowledge and Data Engineering*, 22:1345–1359, 2010.
- [23] Colin Raffel, Noam M. Shazeer, Adam Roberts, Katherine Lee, Sharan Narang, Michael Matena, Yanqi Zhou, Wei Li, and Peter J. Liu. Exploring the limits of transfer learning with a unified text-to-text transformer. *ArXiv*, abs/1910.10683, 2019.
- [24] Francisco Romero, Qian Li, Neeraja J. Yadwadkar, and Christos Kozyrakis. Infaas: Managed & model-less inference serving. *CoRR*, abs/1905.13348, 2019.
- [25] Francisco Romero, Mark Zhao, Neeraja J. Yadwadkar, and Christos Kozyrakis. Llama: A heterogeneous & serverless framework for auto-tuning video analytics pipelines. In *Proceedings of the ACM Symposium on Cloud Computing*, SoCC '21, page 1–17, New York, NY, USA, 2021. Association for Computing Machinery.
- [26] Mark Sandler, Andrew G. Howard, Menglong Zhu, Andrey Zhmoginov, and Liang-Chieh Chen. Inverted residuals and linear bottlenecks: Mobile networks for classification, detection and segmentation. *CoRR*, abs/1801.04381, 2018.
- [27] Haichen Shen, Lequn Chen, Yuchen Jin, Liangyu Zhao, Bingyu Kong, Matthai Philipose, Arvind Krishnamurthy, and Ravi Sundaram. Nexus: a GPU cluster engine for accelerating dnn-based video analysis. In *Proceedings of the 27th ACM Symposium on Operating Systems Principles, SOSP 2019, Huntsville, ON, Canada, October 27-30, 2019*, pages 322–337. ACM, 2019.
- [28] Karen Simonyan and Andrew Zisserman. Very deep convolutional networks for large-scale image recognition, 2014.
- [29] Christian Szegedy, Sergey Ioffe, and Vincent Vanhoucke. Inception-v4, inception-resnet and the impact of residual connections on learning. *CoRR*, abs/1602.07261, 2016.
- [30] Christian Szegedy, Vincent Vanhoucke, Sergey Ioffe, Jonathon Shlens, and Zbigniew Wojna. Rethinking the inception architecture for computer vision. *CoRR*, abs/1512.00567, 2015.
- [31] Mingxing Tan and Quoc V. Le. Efficientnet: Rethinking model scaling for convolutional neural networks. *CoRR*, abs/1905.11946, 2019.

- [32] Mingxing Tan and Quoc V. Le. Efficientnetv2: Smaller models and faster training. *CoRR*, abs/2104.00298, 2021.
- [33] Luping Wang, Lingyun Yang, Yinghao Yu, Wei Wang, Bo Li, Xianchao Sun, Jian He, and Liping Zhang. Morphling: Fast, near-optimal auto-configuration for cloud-native model serving. In *Proceedings of the ACM Symposium on Cloud Computing, SoCC '21*, page 639–653, New York, NY, USA, 2021. Association for Computing Machinery.
- [34] Peifeng Yu and Mosharaf Chowdhury. Fine-grained GPU sharing primitives for deep learning applications. In Inderjit S. Dhillon, Dimitris S. Papailiopoulos, and Vivienne Sze, editors, *Proceedings of Machine Learning and Systems 2020, MLSys 2020, Austin, TX, USA, March 2-4, 2020*. mlsys.org, 2020.
- [35] Chengliang Zhang, Minchen Yu, Wei Wang, and Feng Yan. Mark: Exploiting cloud services for Cost-Effective, SLO-Aware machine learning inference serving. In *2019 USENIX Annual Technical Conference (USENIX ATC 19)*, pages 1049–1062, Renton, WA, July 2019. USENIX Association.
- [36] Barret Zoph, Vijay Vasudevan, Jonathon Shlens, and Quoc V. Le. Learning transferable architectures for scalable image recognition. *CoRR*, abs/1707.07012, 2017.

A Global Partitioning Algorithm

We first present details on the MILP optimization formulation that we use to partition the models across sub-clusters and clusters. We then provide an evaluation of the quality of approximated solutions to the MILP in the context of our system.

A.1 Model formulation

We want to partition m models into l sub-clusters. For each sub-cluster, the maximum dispatcher capability of request rate is R_{\max} , and the maximum memory size of backends is S_{\max} . Let x_{ij} represents whether model i is assigned to sub-cluster j . The request rate, static memory size, dynamic (runtime) memory size of model i are r_i, s_i, d_i respectively. The average request rate per sub-cluster is $\bar{R} = \sum_i r_i / l$. Similarly, the average static memory size per sub-cluster is $\bar{S} = \sum_i s_i / l$. The partitioning problem can be formulated as follows.

$$\text{minimize } \Delta R + w\Delta S \quad (4)$$

$$\text{subject to } \sum_i r_i x_{ij} \leq R_{\max} \quad \forall j \quad (5)$$

$$\sum_i s_i x_{ij} + \max_i d_i x_{ij} \leq S_{\max} \quad \forall j \quad (6)$$

$$\left| \sum_i r_i x_{ij} - \bar{R} \right| \leq \Delta R \quad \forall j \quad (7)$$

$$\left| \sum_i s_i x_{ij} - \bar{S} \right| \leq \Delta S \quad \forall j \quad (8)$$

$$\sum_j x_{ij} = 1 \quad \forall i \quad (9)$$

$$x_{ij} \in \{0, 1\} \quad \forall i, j \quad (10)$$

(9) and (10) represent that each model is assigned to exactly one sub-cluster. (5) requires that the request rate of each sub-cluster is less than the maximum dispatcher capability. (6) requires that the static memory size plus the maximum dynamic (runtime) memory size is less than the maximum memory size of backends. (7) and (8) denote that each sub-cluster's request rate and static memory size should be close to the averages. Therefore, our objective (4) is to minimize the differences to the averages as much as possible. The parameter w is a coefficient that balances the request rate and model memory size.

Disruption Minimization The above model can generate an initial assignment when the system starts. When the system is running, we would like to generate the next assignment considering the current assignment, so the disruption is minimized.

Given the current assignment matrix X' where x'_{ij} denotes whether model i is currently put into sub-cluster j . Let c_{ij} denote the cost for loading/unloading model i to/from sub-cluster j (assuming the cost is symmetric between loading and unloading). The maximum allowed cost is C_{\max} . Let y_{ij} represent whether there is a change for model i and sub-cluster j as $y_{ij} = |x_{ij} - x'_{ij}|$. To bound the total cost of change within C_{\max} , we have

$$\sum_i \sum_j c_{ij} y_{ij} \leq C_{\max}. \quad (11)$$

Practical Implementation As solving general MILP problems is NP-hard, an optimal solution of the above model can not be obtained within a reasonable amount of time. Therefore, we need to use an approximated solution obtained within a time bound. Based on our testing with CPLEX solver and a running time of 10 seconds for $m = 400$ and $l = 4$, an approximate solution is significantly better than any randomly generated assignments.

A.2 Effectiveness of Cluster Partitioning

We next evaluate the effectiveness of the MILP partitioning model for partitioning the models and the workload across sub-clusters or clusters. We created a random solver as a baseline. The random solver will simply generate a random partition, check it against all the constraints, evaluate using the MILP objective, and repeat. It will output the partition with the least objective that satisfies all the constraints within a time constraint. Similarly, we use a solver to tackle the MILP problem and impose the same time limit for the solver (which is 10 seconds in our current system) to get the best solution so far.

We generate multiple configurations to represent different scenarios. Each configuration contains a random selection of models from our model zoo, where we generate multiple variants as specialized instantiations of a given model. We consider large-scale partitioning problems that partitions 800 models across 20 partitions. The request rate for each model is assumed to be independent and draw from an exponential distribution. We measure the goodness of a partition based on the imbalance factors for memory and load. The imbalance factor is defined as $\frac{\max - \min}{\text{avg}}$ across the different partitions generated by the algorithm. We compute the imbalance factor for both static memory and request rate across all dispatchers / subclusters. The smaller the imbalance metric, the better is the partition. Figure 15 depicts the CDF of the imbalance factors for memory and load across the different experiments. We observe that our MILP-based algorithm provides load-balanced partitions within our time window of 10 seconds, which makes it appropriate for epoch-level reconfigurations that happen every few minutes.

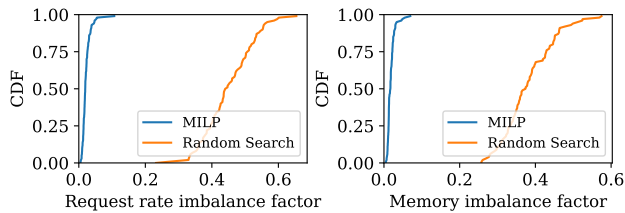


Figure 15: Evaluating the effectiveness of MILP search for the partitioning problem

B Model Zoo Details

Table 5 and Table 6 show the profiles of models used in the evaluation section for 1080Ti and A100 respectively. Latency SLO associated with each model ensures that each model can run with batch size greater than or equal to 4.

Name	α (ms)	β (ms)	β/α	SLO
NASNetMobile	0.570	14.348	25.172	33ms
MobileNetV3Small	0.335	5.350	15.970	20ms
DenseNet169	1.271	13.618	10.714	37ms
DenseNet121	1.061	10.312	9.719	29ms
DenseNet201	1.733	15.687	9.052	45ms
EfficientNetV2B0	1.006	7.493	7.448	23ms
MobileNetV3Large	0.820	5.256	6.410	20ms
InceptionV3	1.964	8.771	4.466	33ms
EfficientNetV2B1	1.661	7.247	4.363	27ms
ResNet50V2	1.409	5.947	4.221	23ms
ResNet152V2	3.471	13.049	3.759	53ms
ResNet101V2	2.438	9.095	3.731	37ms
InceptionResNetV2	5.090	18.368	3.609	77ms
EfficientNetB0	1.569	5.586	3.560	23ms
MobileNetV2	1.180	3.483	2.952	20ms
ResNet101	3.164	9.065	2.865	43ms
EfficientNetB1	2.489	6.674	2.681	33ms
ResNet50	2.050	5.378	2.623	27ms
EfficientNetV2B2	2.254	5.896	2.616	29ms
VGG19	3.059	7.857	2.568	40ms
ResNet152	4.599	11.212	2.438	59ms
MobileNet	1.009	2.390	2.369	20ms
VGG16	2.734	5.786	2.116	33ms
EfficientNetB2	3.446	5.333	1.548	38ms
EfficientNetV2B3	4.072	5.981	1.469	44ms
NASNetLarge	17.656	18.952	1.073	179ms
EfficientNetV2S	8.463	8.862	1.047	85ms
EfficientNetB3	5.924	4.849	0.819	57ms
EfficientNetV2L	40.313	28.208	0.700	378ms
EfficientNetV2M	22.619	14.786	0.654	210ms
EfficientNetB5	23.435	10.301	0.440	208ms
Xception	4.751	2.046	0.431	42ms
SSDMobilenet	23.778	9.729	0.409	209ms
EfficientNetB4	12.088	4.412	0.365	105ms
BERT	7.008	0.159	0.023	56ms

Table 5: Model profiles on an NVIDIA 1080Ti.

Name	α (ms)	β (ms)	β/α	SLO
DenseNet121	0.054	10.546	195.296	21ms
DenseNet201	0.304	14.345	47.188	31ms
DenseNet169	0.289	13.365	46.246	29ms
ResNet50V2	0.135	5.560	41.185	20ms
EfficientNetB0	0.115	4.326	37.617	20ms
ResNet101	0.284	8.266	29.106	20ms
ResNet152	0.390	10.449	26.792	24ms
ResNet101V2	0.391	8.219	21.020	20ms
MobileNetV3Large	0.196	4.072	20.776	20ms
EfficientNetB1	0.291	5.797	19.921	20ms
ResNet50	0.268	5.172	19.299	20ms
ResNet152V2	0.589	10.054	17.070	24ms
MobileNetV2	0.190	2.892	15.221	20ms
EfficientNetV2B3	0.543	7.596	13.989	20ms
InceptionResNetV2	1.112	15.27	13.732	39ms
EfficientNetV2B1	0.443	5.929	13.384	20ms
NASNetMobile	0.536	6.860	12.799	20ms
EfficientNetV2B0	0.377	4.272	11.332	20ms
EfficientNetB2	0.520	5.333	10.256	20ms
MobileNetV3Small	0.315	3.211	10.194	20ms
InceptionV3	0.913	6.732	7.373	20ms
MobileNet	0.285	1.901	6.670	20ms
EfficientNetV2S	1.454	7.378	5.074	26ms
EfficientNetV2B2	0.901	4.532	5.030	20ms
VGG16	0.660	2.252	3.412	20ms
EfficientNetB3	1.239	4.205	3.394	20ms
Xception	0.801	2.638	3.293	20ms
VGG19	0.893	2.181	2.442	20ms
NASNetLarge	3.464	7.154	2.065	42ms
EfficientNetV2M	4.479	6.861	1.532	49ms
EfficientNetB4	2.881	4.103	1.424	31ms
EfficientNetV2L	7.520	6.675	0.888	73ms
EfficientNetB5	6.121	2.283	0.373	53ms
SSDMobilenet	19.448	4.442	0.228	164ms
EfficientNetB6	9.754	1.984	0.203	82ms
EfficientNetB7	16.339	2.751	0.168	136ms
BERT	7.353	0.222	0.030	59ms

Table 6: Model profiles on an NVIDIA A100.

C Scheduling Algorithm Pseudocode

```

struct Candidate: bs, exec_at, invalid_after
def delay(bs): return d_ctrl + d_data * bs
class ModelThread:
    model: ModelID
    batch: BatchPolicy
    drop_timer: Timer
    c: Optional[Candidate]

# Frontend -> ModelThread
def schedule(req):
    batch.enqueue(req)
    update_candidate(-inf)
    rank_thread.inform_candidate(model, c)

# RankThread -> ModelThread
def granted_gpu(gpu, gpu_free_at):
    update_candidate(gpu_free_at)
    if c is None:
        free_at = max(now(), gpu_free_at)
    else:
        inputs = batch.pop_inputs()
        send(gpu, ExecutionMsg(inputs, c.exec_at))
        free_at = c.exec_at + exec_elapse(len(inputs))
        update_candidate(-inf)
    rank_thread.inform_gpu(gpu, free_at)
    rank_thread.inform_candidate(model, c)

def update_candidate(gpu_free_at):
    batch.update_batch(gpu_free_at)
    bs = len(batch.inputs)
    if bs > 0:
        dl = batch.inputs[0].deadline
        drop_timer.cancel()
        drop_timer.set(dl, lambda: update_candidate(-inf))
        earliest = max(now()+delay(bs), gpu_free_at)
        frontrun_at = dl - exec_elapse(model, bs+1)
        beta_lambda = calculate_beta_lambda()
        exec_at = bs > beta_lambda ? earliest : frontrun_at
        exec_at = max(earliest, frontrun_at)
        invalid_after = dl - exec_elapse(model, bs)
        c = Candidate(bs, exec_at, invalid_after)
    else:
        c = None
    for req in batch.pop_dropped():
        send(req.frontend, QueryDroppedMsg(req))

class RankThread:
    gpu_free_at: Map[GpuID, TimePoint]
    gpu_timer: Map[GpuID, Timer]
    model_timer: Map[ModelID, Timer]
    mc: Map[ModelID, Candidate]

# ModelThread -> RankThread
def inform_candidate(m: ModelID, c: Optional[Candidate]):
    del mc[m]
    model_timer[m].cancel()
    if c is not None:
        model_timer[m].set(c.exec_at-delay(c.bs),
            lambda: on_model_timer(m, c))

# ModelThread -> RankThread
def inform_gpu(gpu: GpuID, free_at: TimePoint):
    gpu_free_at[gpu] = free_at
    set_gpu_timer()

def on_model_timer(m: ModelID, c: Candidate):
    gpu, free_at = gpu_free_at.get_earliest()
    if free_at <= c.exec_at:
        gpu_free_at[gpu] = +inf
        model_thread[m].granted_gpu(gpu, free_at)
    else:
        mc[m] = c
        set_gpu_timer()

def set_gpu_timer():
    gpu, free_at = gpu_free_at.get_earliest()
    gpu_timer[gpu].cancel()
    if len(mc) > 0:
        m, c = mc.get_by_max_delay()
        gpu_timer[gpu].set(free_at-delay(c.bs),
            lambda: on_gpu_timer(gpu))

def on_gpu_timer(gpu: GpuID):
    free_at = gpu_free_at[gpu]
    Remove (m,c) from mc where free_at > c.invalid_after
    if len(mc) > 0:
        m, c = mc.get_by_earliest_exec_at()
        model_thread[m].granted_gpu(gpu, free_at)
    set_gpu_timer()

```

Figure 16: Pseudo-code of the scheduling algorithm.